Isomerism-governed Molecular Electrocatalysis

A Thesis

submitted to

Indian Institute of Science Education and Research Pune in partial fulfilment of the requirements for the BS-MS Dual Degree Programme

by

Vishnupriya G Kumar

Reg. No. 20161113

Department of Chemistry

Indian Institute of Science Education and Research Pune

Dr. Homi Bhabha Road,

Pashan, Pune 411008, INDIA.

October, 2021

Supervisor: Dr. Muhammed Musthafa

Certificate

This is to certify that this dissertation entitled ***"Isomerism-governed Molecular Electrocatalysis"*** towards the partial fulfilment of the BS-MS dual degree programme at the Indian Institute of Science Education and Research, Pune represents study/work carried out by Ms. Vishnupriya G Kumar (Reg. No. 20161113) at Indian Institute of Science Education and Research under the supervision of Dr. Muhammed Musthafa, Associate Professor, Department of Chemistry, during the academic year 2020-2021.

Dr. Muhammed Musthafa

Committee:

Dr. Muhammed Musthafa (Supervisor)

Dr. Partha Hazra (TAC)

This thesis is dedicated to my parents

Declaration

I hereby declare that the matter embodied in the report entitled ***"Isomerism-governed Molecular Electrocatalysis"*** are the results of the work carried out by me at the Department of Chemistry, Indian Institute of Science Education and Research, Pune, under the supervision of Dr. Muhammed Musthafa and the same has not been submitted elsewhere for any other degree.

Vishnupriya G Kumar

Date: 30/10/2021

Table of Contents

List of Figures

Abstract

N_4-macrocyclic molecules such as metal phthalocyanines and metal porphyrins (MN_4 electrocatalysts) have been vastly investigated as viable non-precious molecular electrocatalysts for a wide range of electrochemical applications due to their fast redox processes, chemical and thermal stabilities, and highly tuneable optoelectronic properties. The influence that the functionalization in the secondary sphere exerts on their electrocatalysis and electronic structure is well studied. However, the effect of positional isomerism of the functional group on activity is much less explored. This work focuses on the role of isomerism of the amino functional group in the electrocatalytic activity of regioisomers of amino-substituted cobalt phthalocyanine functionalized at the α- and β- positions on the N4 macrocycle of the molecule. The synthesized electrocatalysts were anchored onto CNT support and the same was confirmed by various spectroscopic characterization. These TACoPc/CNT composites were probed for their activity towards the oxidation of hydrazine since it is a commonly used liquid fuel alternative for hydrogen in fuel cells. The β-TACoPc isomer was found to be a better catalyst than α-TACoPc and exhibited better performance in Hydrazine-Oxygen fuel cell. However, the α-TACoPc fuel cell showed more durability.

Acknowledgements

First of all, I would like to express my wholehearted and profound gratitude to my supervisor Dr. Muhammed Musthafa O. T., Associate Professor, Department of Chemistry, IISER Pune, for giving me the chance to work on my thesis project under his supervision and providing guidance and unconditional support during this whole time. I am very thankful for the inputs my TAC member Dr. Partha Hazra, has given during the project.

I want to extend my sincere gratitude to all the teaching and non-teaching staff of the Department of Chemistry, IISER Pune, who has directly or indirectly helped me during my time here. I am incredibly grateful to my lab seniors, K Alagar Raja, Sanchayita Mukhopadhyay and Zahid Manzoor Bhat, for their invaluable counsel and knowledge that helped me a lot. I greatly appreciate all my lab members for their support, advising me throughout the project as well as creating a lively working environment.

I am immensely grateful for my family, for their love and continuous encouragement throughout all these years, without which I'd never have achieved anything. Finally, I would like to thank each of my friends who have been a constant source of support and cheer in my life.

Chapter 1 : Introduction

1.1. N_4 Macrocycles

Molecules with the N_4 macrocyclic framework such as metallophthalocyanines, metalloporphyrins, and analogous molecules (MN_4 electrocatalysts) anchored on carbon and graphitic support have been investigated as non-precious molecular electrocatalysts for an extensive array of electrochemical applications owing to their thermal and chemical stabilities and highly tuneable optoelectronic properties [1,2]. Such molecular catalysts are preferred over conventional metal-based electrocatalysts, since their electrocatalytic activity can be tuned by altering the central metal ion and the functional groups. In contrast, the activity of metal-based catalysts is modified by several processes such as engineering the surface area to volume ratio, foreign metal doping, modifying synthesis method or polishing to expose reactive crystal planes, etc. [2]. MN_4 complexes have fast redox processes involving minimal reorganizational energies and hence play the role of excellent redox mediators in electron transfer reactions of numerous substrates [3].

The influence over the catalytic activity and the electronic structure of the molecular electrocatalysts, exerted by derivatization in the secondary sphere has been well explored. For instance, tetrasulphonated cobalt phthalocyanine was studied as a bifunctional electrocatalyst that catalyses both oxygen reduction reaction (ORR) and oxygen evolution reaction (OER) (Chuan Li et al., 2019) [4]. Marc et al., in 2019, reported a Trimethyl ammonium substituted CoPc electrocatalyst for highly selective CO_2 reduction with good current density matching noble metal-based catalysts [5]. The substitution modifies the electron density distribution at the central metal atom, which is the active site for electron transfer, altering the catalytic activity [2].

Although extensive research has been done in MN4 electrocatalysts with respect to substitution, our group is the first to investigate the effect of isomerism of the functional group in molecular electrocatalysts [6,7]. The effect of the position of functionalization on the electrocatalytic activity has been studied by our group using different electrochemically and environmentally significant reactions, such as oxygen reduction reaction (ORR), Arsenic oxidation, Water oxidation, etc. [7]. This work focuses on how isomerism affects the electrocatalytic activity of Tetraamino Cobalt Phthalocyanine towards hydrazine oxidation. In this regard, we have synthesised regioisomers of amino-substituted cobalt phthalocyanine conferred at the α- and β-carbons on the N_4 macrocycle (Figure 1).

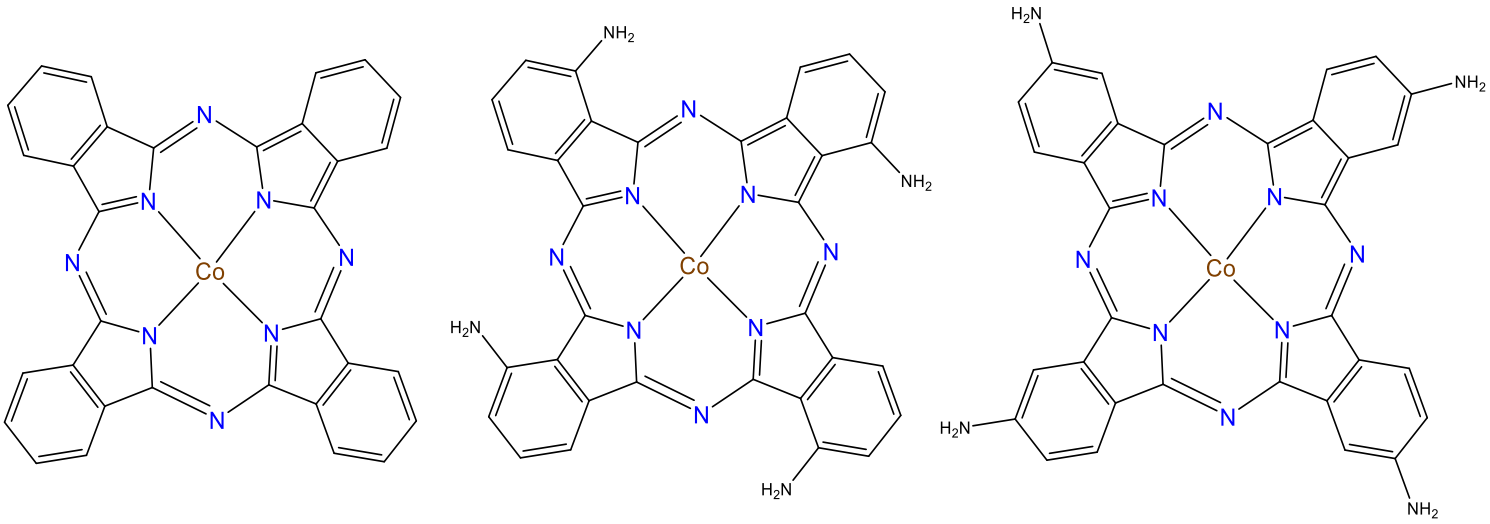

Figure 1 Chemical structure of Cobalt Phthalocyanine, α-TetraaminoCoPc and β-TetraaminoCoPc

This effect is mainly studied in terms of onset potential and peak current on the voltammogram of the reaction for each catalyst. Onset potential is the potential at which the reaction starts occurring on the electrode surface.

1.2. Hydrazine Oxidation

Hydrazine has a significant role in various industrial processes. It has been widely used as an anti-corrosion agent in nuclear as well as traditional electric power plants. Even though contact with small amounts of hydrazine is not fatal, long-term exposure to the compound can damage the liver, central nervous system, kidneys. It is often a contaminant in water bodies due to discharge from industrial plants. Thus, the electrochemistry of hydrazine and its detection is of interest in a number of areas. Explosives also make use of this compound since it combines with oxygen exothermally to produce nitrogen. Hydrazine is also used as a fuel molecule since its combustion produces a lot of energy. It is especially studied as a substitute for hydrogen in fuel cells since it is a liquid at room temperature and can be handled more easily. It has been applied in developing high power density direct hydrazine-air fuel cells.

1.3. Fuel Cell

A fuel cell is an electrochemical energy conversion device that turns the chemical energy from the reaction occurring at the electrode-electrolyte interface into electrical energy. The chemical reaction (redox reaction) happens at the two electrodes in the fuel cell – oxidation at the anode and reduction at the cathode. Fuel is continuously supplied from both sides of the electrodes. The chemical energy generated from the oxidation or reduction of the fuel is transformed into electrical energy. There are different fuel cells based on what electrolytes are used for ionic conductance which

connects the electrodes, closing the electrical circuit. The electrolyte can be a liquid, like alkali, or a solid, like polymer or solid oxide. Some examples of fuel cells are proton exchange membrane fuel cell (PEMFC), solid oxide fuel cell, molten carbonate FC, phosphoric acid FC, alkaline FC etc.

Proton Exchange Membrane Fuel Cells (PEMFCs), among these, are energy conversion devices at a higher efficiency with a near zero emission [8,9,10]. A Proton Exchange Membrane Fuel Cell (PEMFC) converts the chemical energy of H_2 and O_2 into electricity. The H_2 gas being supplied gets oxidised at the anode to form H+, which migrates across the membrane, and electrons removed from H_2 travel through the external circuit to the cathode, where it combines with O_2 and H^+ forming water. [11] It has zero emission and is environmentally friendly because the end product is water, and no harmful gases are released. State of the art PEMFC uses platinum-based electrocatalysts to drive the reactions at the current density required. Since platinum is a very costly precious metal, exploring alternative electrocatalysts that are non-precious in nature is favourable.

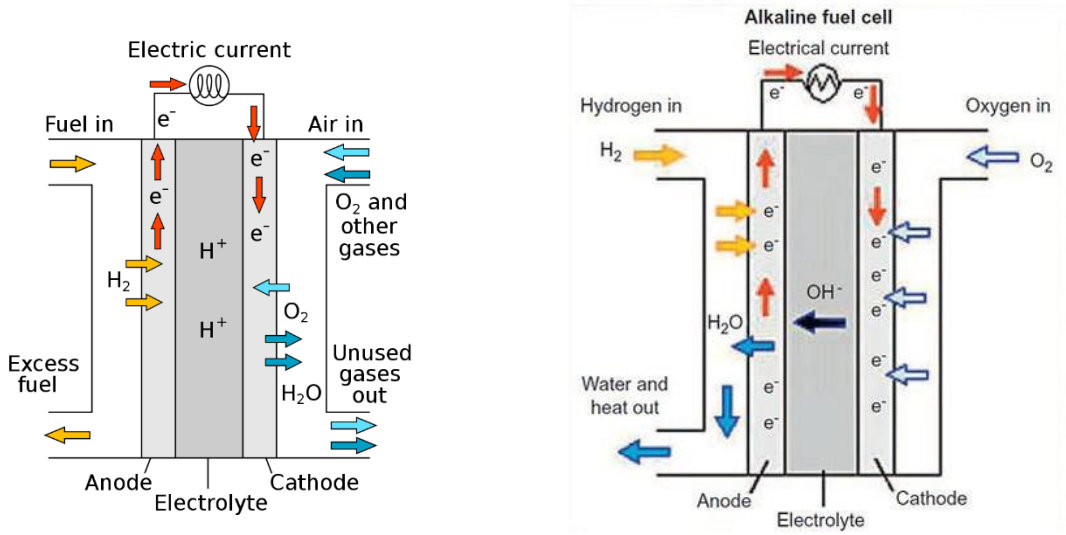

Figure 2 Schematic diagram of (A)PEM Fuel Cell, (B)Alkaline Fuel Cell

H_2 gas, being highly explosive, presents challenges in storage and safe handling. So fuel cells using liquid fuels like alcohol and borohydride have been explored in literature[12] due to their various beneficial features such as high energy density, the feasibility for operating at remote locations (including space), enhanced efficiency (particularly in comparison to combustion engines), and an abundance of liquid fuels. Direct hydrazine air fuel cells (DHAFC) have been of interest in this regard since hydrazine is a toxic pollutant and it gets converted to N_2 upon oxidation. DHAFC also uses Pt electrocatalyst, which is an expensive precious metal, on both electrodes- for hydrazine oxidation as well as oxygen reduction. In this work, we are using our

synthesized Tetraamino Cobalt Phthalocyanine isomeric electrocatalyst as anode for hydrazine oxidation.

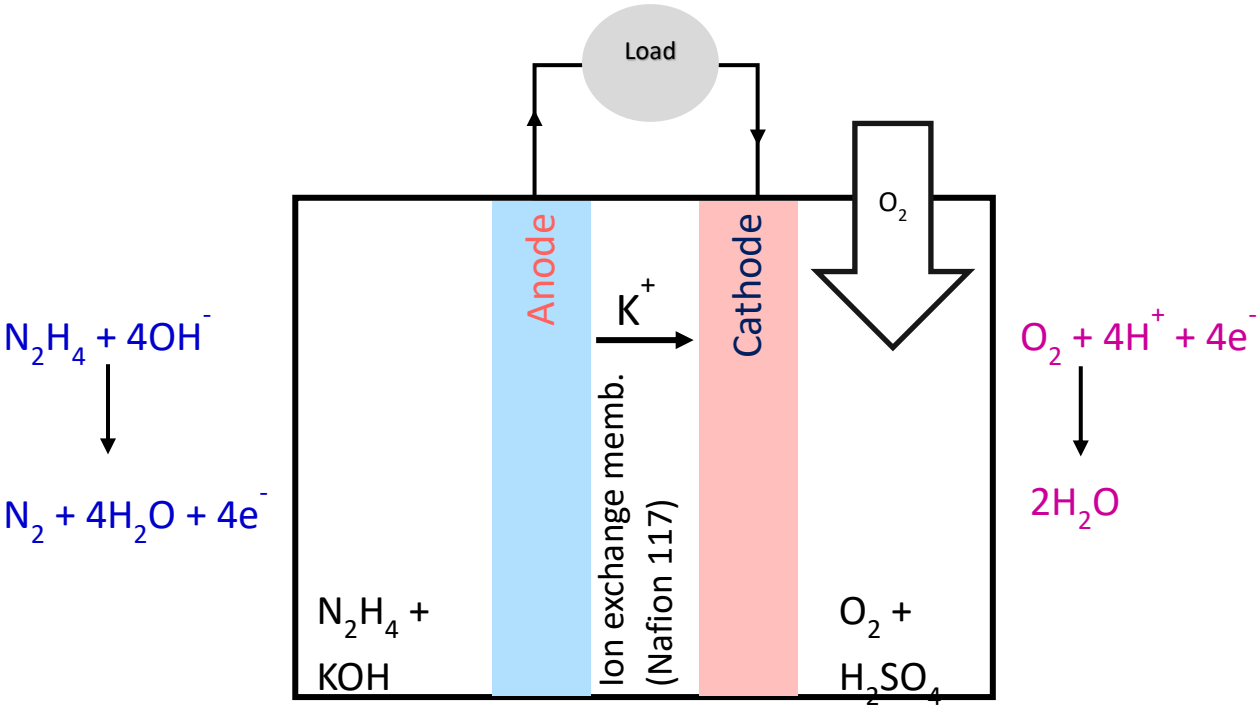

Figure 3 Schematic diagram of Hydrazine-air fuel cell

We have utilised acid in the cathodic compartment and alkali in the anodic compartment since it has been shown that the acid-base neutralization energy can be converted electrochemically to electricity, thereby enhancing the cell performance [13].

Chapter 2 : Materials and Methods

2.1 Chemicals

The chemicals such as sulfuric acid (96 %), dimethyl formamide (DMF) (99 %), 3-nitro phthalimide (98 %), 4-nitro phthalimide (98 %), ethanol (95 %), isopropyl alcohol (99 %), ammonium molybdate (99.99 %), ammonium chloride (≥98 %), urea (98 %), nitrobenzene (99 %), toluene (99.5 %), hexane (95 %), methanol (99 %), were purchased from Alfa Aesar India. The carbon nanotubes (CNTs) were acquired from C-Nano (FT 9000). H2O2 solution (30%), Cobalt(II) Chloride hexahydrate (≥98 %) and Nafion (5 wt.%) solution were purchased from Sigma-Aldrich, India. Analytical grade potassium chloride (99.8%), Hydrazine hydrate (78-82%), and potassium hydroxide (85 %) were obtained from Rankem. Pt/C was obtained from Johnson Matthey, India. Nafion 117 membrane was procured from Ion Power (USA).

2.2 Synthesis of Catalyst

2.2.1 Synthesis of 1,8,15,22 -Tetraaminophthalocyanatocobalt (II) (α-TACoPc), 2,9,16,23 -Tetraaminophthalocyanatocobalt (II) (β-TACoPc), and Phthalocyanatocobalt (II) (CoPc)

The synthesis of 1,8,15,22-Tetraamino Cobalt Phthalocyanine (α-TACoPc) / 2,9,16,23-Tetraamino Cobalt Phthalocyanine (β-TACoPc) was performed according to previous literature [6,7]. First, the nitro substituted CoPc isomers were synthesized, which were reduced to yield the amino-substituted CoPc isomers.

3-nitro phthalimide / 4-nitro phthalimide (3.86 g), urea (6.0 g), ammonium molybdate (0.05 g), and ammonium chloride (0.5 g) were ground and put into 30 mL of nitrobenzene in a 250 mL RB flask which was then stirred for 10 minutes to get a homogeneous mixture. Cobalt(II) chloride hexahydrate (1.2 g) was added to this, and the mixture was stirred vigorously at 100˚C for about 30 minutes. The temperature of the reaction mixture was ramped up to 180˚C at a rate of 10˚C / 30 minutes and afterwards kept at 180˚C for about 4 hours while refluxing the reaction mixture. The mixture was then diluted with toluene (50 mL), and the resulting precipitate was filtered, washed thoroughly with hot water and methanol and finally washed with hexane and afterwards dried in an oven at 80˚C. For the synthesis of CoPc, nitro phthalimide was replaced with phthalimide and the same procedure was followed.

The Tetra nitro Cobalt Phthalocyanine (0.75 g), synthesized as above, was taken in a 250mL round bottom flask along with sodium sulphide nonahydrate (3.0 g) and 30 ml of N,N-dimethyl formamide and heated to 80° C for about 2 hours [14]. After it had cooled down to room temperature, the mixture was diluted with ice water (200 ml), and the resulting precipitate was filtered out and washed thoroughly with hot water, methanol, and hexane in that order [14]. The obtained precipitate was dried in an oven to obtain 2,9,16,23-Tetraamino Cobalt phthalocyanine or 1,8,15,22-Tetraamino Cobalt phthalocyanine that was used for experiments. The as-synthesized

molecules were thoroughly characterized with different spectroscopic techniques. (See chapter 3 for details)

2.2.2 Synthesis of CoPc, α-TACoPc and β-TACoPc anchored on CNTs

The pre-treatment of CNTs was carried out by calcining them at 500°C in air for five hours. After cooling, they were put in a 5 wt.% HCl aqueous solution and sonicated for 30 minutes [23]. The resulting solution was filtered to obtain the pure CNTs, which were then washed with ultrapure water over 10 times. CoPc and TACoPc isomers were anchored over CNT by mixing known amounts of CNT and TACoPc in the stoichiometric ratio of 2:1 (w/w) in DMF and sonicated for about 30 minutes to attain a well-mixed suspension [15]. This suspension was then kept for stirring at ambient temperature for 24 h. Subsequently, this mixture was centrifuged, and the resulting precipitate was washed with DMF and ethanol. Ultimately, the washed precipitate was lyophilized to get the final composite catalyst, which was then characterized by various spectroscopic techniques.

2.3 Characterization Techniques

2.3.1 Ultra-violet visible spectroscopy

When UV-visible radiation is incident on a molecule, it will absorb radiation of a particular wavelength and undergo an electronic transition from occupied molecular orbital to higher energy unoccupied molecular orbitals (HOMO→LUMO) [16]. The information about the energy gap related to functional group can be obtained from the wavelength of light corresponding to the peaks in the absorbance spectra.

According to Beer-Lambert law,

$$A = \varepsilon C l$$

where A = absorbance, ε = molar extinction coefficient (L mol^{-1} cm^{-1}), C=concentration of molecule (mol /L), l = path length (cm)

UV visible spectroscopy was used to collect the UV-Vis spectra of the synthesized catalysts- CoPc, α-TACoPc, β-TACoPc, and their respective composite material with carbon nanotubes. Samples were dissolved in N, N-dimethyl formamide. UV-visible measurements were carried out in 3mL quartz cuvettes using a Perkin Elmer Lambda 950 spectrophotometer.

2.3.2 Infrared spectroscopy

IR spectroscopy is helpful to detect or distinguish a particular kind of bond or functional group. FTIR spectroscopy was performed to characterize the functionalization of catalysts and confirm their formation. ATR-FTIR (Bruker Alpha FTIR Spectrometer) was used to collect the FTIR data.

2.3.3 Raman Spectroscopy

Raman spectroscopy detects the inelastic scattering of light to determine the vibrational modes of a molecule. The Raman spectra of the synthesized catalysts were

obtained using a Raman microscope (LabRAM HR, Horiba Jobin Yvon). Samples were prepared by sonication of catalysts in isopropanol and drop-casting them onto a glass slide.

2.3.4 NMR Spectroscopy

Proton NMR spectroscopy was used to differentiate the α and β isomers of TACoPc. NMR spectra for the samples were recorded on a 400 MHz Jeol ECS-400 and Bruker 400 MHz instruments.

2.3.5 Field Emission Scanning Electron Microscopy (FESEM)

SEM images and EDX analysis were carried out using an Ultra Plus Field Emission Scanning Electron Microscope with integral charge compensator and embedded EsB and AsB detectors. Oxford Xmax instruments 80mm^2. (Carl Zeiss NTS, Gmbh), Imaging conditions: 2kV, WD= 2mm, 200kX, In-lens detector. Catalysts were sonicated in IPA for 2 hrs. The dispersion was drop-casted on copper foil and then dried under light.

2.3.6 Cyclic voltammetry

Electrochemical characterization was performed using the VMP300 Electrochemical Workstation (Biologic, France).

A cyclic voltammogram (CV) is the resulting current vs potential curve recorded at the working electrode (the electrode where the reaction monitored takes place) when an excitation potential is applied across it [17]. It is performed using a three-electrode setup which consists of a working electrode, a reference and a counter electrode. The working electrode (WE) potential is monitored with respect to the reference electrode (RE). The excitation potential is linearly varied with time at a specific scan rate (in volts/second) from an initial potential to a vertex potential and then back to the initial potential.

The experiments were done in a standard three-electrode setup with a glassy carbon (3 mm diameter) as working electrode, platinum disc counter electrode and an Ag/AgCl (3.5 M KCl) as reference. The TACoPc-CNT composite was sonicated in IPA with 5 wt.% Nafion binder and drop-casted onto the glassy carbon working electrode in order to investigate electrocatalytic activity. The working electrodes were all manually polished with 0.05-micron alumina powder and then cleaned electrochemically in 0.5 M H_2SO_4. The supporting electrolyte used was 0.1M KOH. The cell was purged with N_2 prior to the experiment for 15 minutes.

2.3.7 Chronoamperometry

Chronoamperometry measures the current as a function of time while a constant voltage is applied on the working electrode with respect to a reference electrode. The electrode is held at a potential at which no faradaic process occurs prior to the experiment; then the potential is stepped to a value at which a redox reaction occurs. The time of initiation of the potential step is defined as zero time. It was used to check the stability of the catalyst by monitoring the current response.

2.4 Fuel Cell assembly

Pre-treatment of Nafion membrane: A Nafion117 membrane was pre-treated by heating in a solution of H_2O_2 and water taken in 1:3 ratio, respectively. It was heated at 80°C for 30 minutes. After washing with distilled water, the membrane was again heated at 80°C in 0.5 M H_2SO_4 solution for 30 minutes [18].

Hydrazine-ORR fuel cell was assembled with the synthesized electrocatalyst as anode and Pt/C based electrode as cathode. The corresponding catalyst ink was made by sonicating TACoPc-CNT isomer (10 mg) in isopropanol and 5 wt.% Nafion binder for 30 minutes; this ink was coated onto Toray carbon paper. Similarly, Pt/C catalyst ink (5 mg per cm^2) was coated onto Pt-loaded carbon paper to make the cathode. A pre-treated Nafion 117 membrane was used between the two electrodes. The electrolytes used were 6 M Hydrazine in 1 M KOH in the anodic compartment and 2 M H_2SO_4 in the cathodic compartment. The anodic compartment was saturated with N_2 gas and the cathodic compartment was purged continuously with O_2.

Chapter 3 : Characterization of catalyst

3.1 Pristine Tetraamino Cobalt Phthalocyanine Isomers

The synthesized molecular electrocatalysts were characterized by various spectroscopic techniques. Matrix-Assisted Laser Desorption Ionization Time-Of-Flight mass spectrometry (MALDI-TOF) gave the characteristic m/z peaks suggesting the successful formation of CoPc, α-TACoPc and β -TACoPc as shown in Figure.

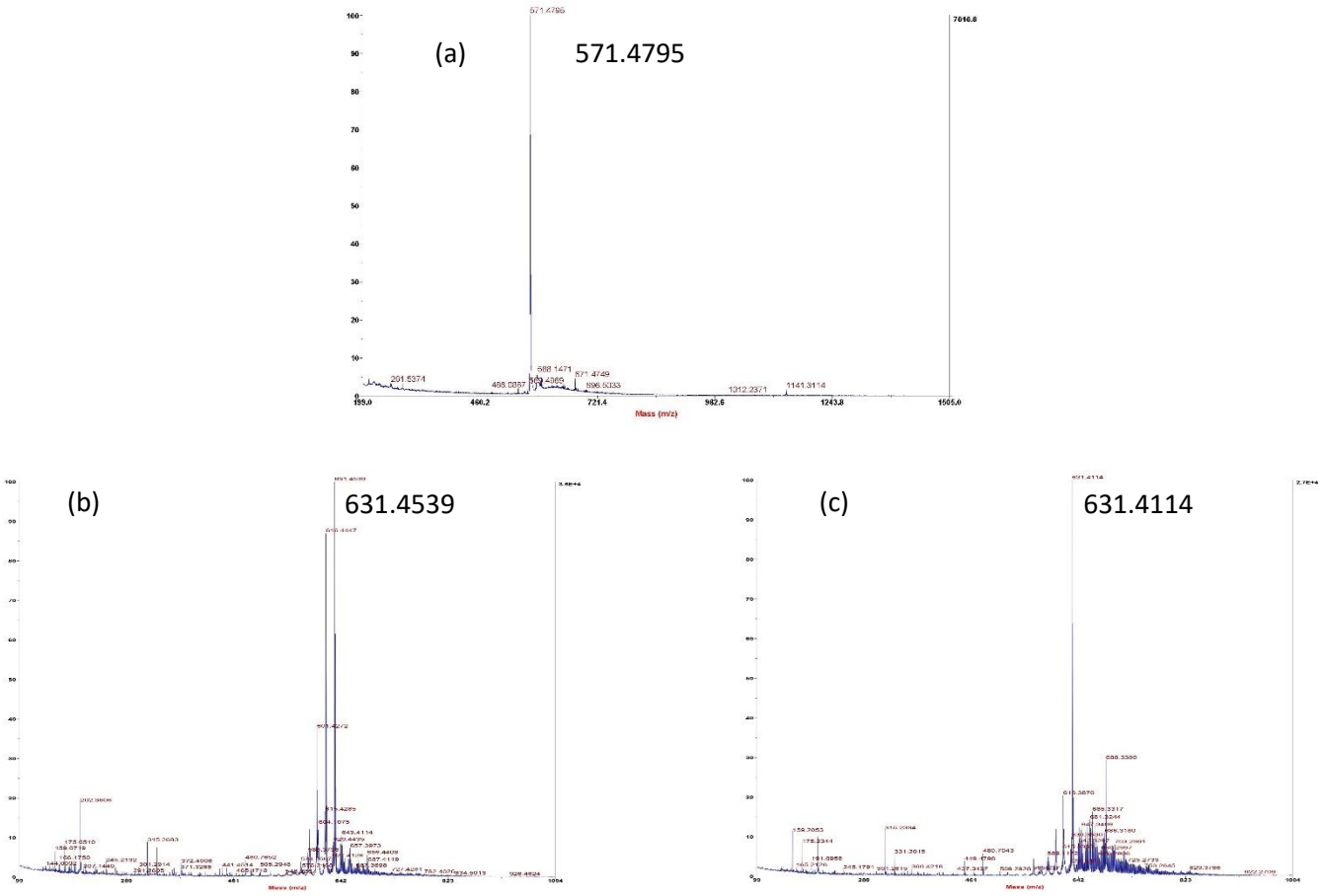

Figure 4 Matrix-assisted laser desorption ionization time-of-flight mass spectrometry (MALDI-TOF) of (a) CoPc, (b) β-TACoPc isomer and (c) α-TACoPc isomer

The UV−vis spectra (Figure 5(a)) shows a B-band (Soret band) and a Q-band in the range of 280−400 nm and 580−800 nm respectively, which are characteristic of a phthalocyanine ring, which can be seen in the spectra of Tetraamino substituted as well as unsubstituted CoPc [19,20]. The low-intensity broad shoulder peak around 430-480 nm corresponds to ligand to metal charge transfer [19]. The regioisomerism of the $-NH_2$ group would be expected to influence the Q-band since it has been discovered to have more ligand characteristics. The absorption maxima of α-isomer are relatively red-shifted with respect to β-isomer and CoPc, implying that it has better electronic delocalization.

The FTIR spectra (Figure 5(b)) of the tetraamino cobalt phthalocyanines indicates the presence of the vibrational frequencies' characteristic to primary aromatic amines-N-H bond stretching vibrations at 3190-3300 cm^{-1} and the in-plane bending vibration of the N-H bond at 1600-1605 cm^{-1}, which are absent in unsubstituted CoPc [20]. Other characteristic features of the aryl amino substituent, like the stretching vibrations of the C-N bond around 1250-1340 cm^{-1} and the out-of-plane deformations of the N-H bond at approximately 700-950 cm^{-1}, seem to be coinciding over the characteristic vibrational bands of the phthalocyanine macrocycle [20].

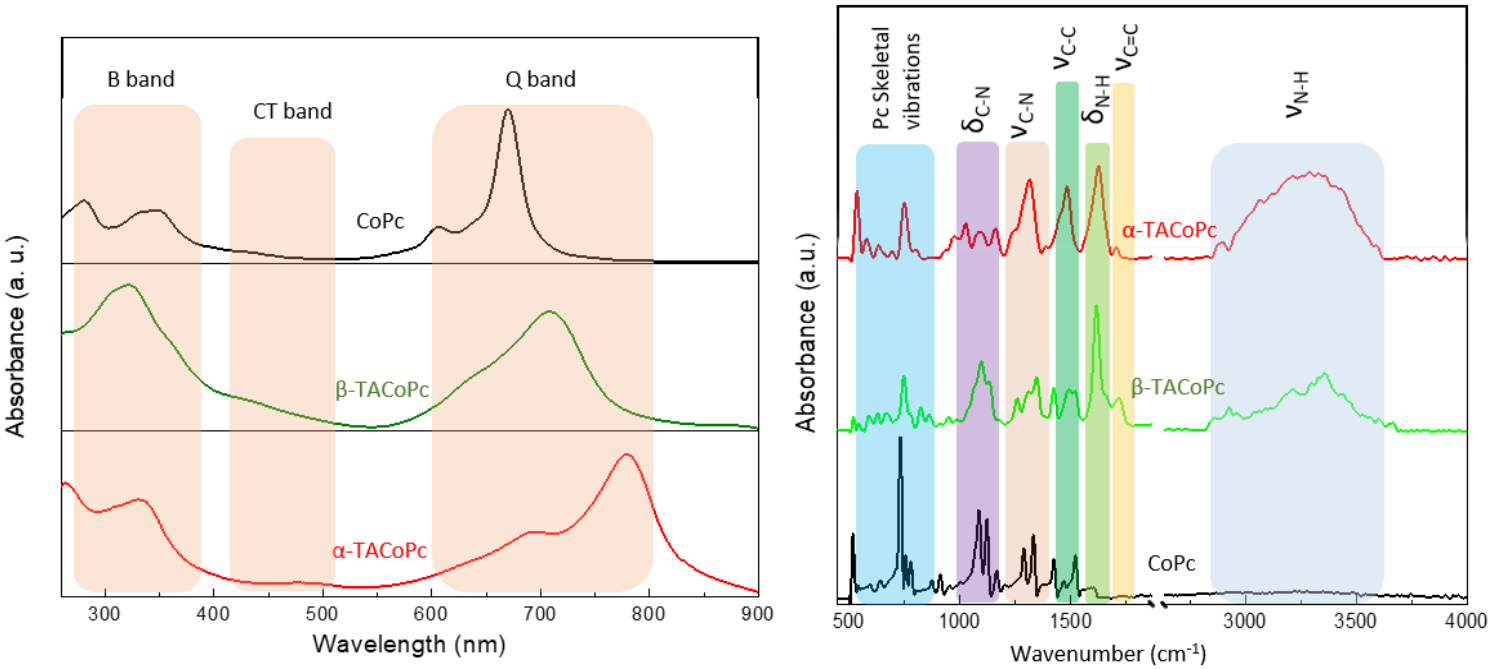

Figure 5 (a)UV-vis spectra and (b) FTIR spectra of CoPc, α-TACoPc and β-TACoPc

The signal between 400 cm^{-1} and 580 cm^{-1} (Figure 6) shows the vibrational mode for C−C−C in-plane bending, and the bands at ~760 cm^{-1} signify the stretching vibrations of the macrocycle. The Raman spectral peaks at 1150-1170 cm^{-1} correspond to the C−H bond bending vibrations [20,21]. The Raman signal at ~1200 cm^{-1} corresponds to the C−H in-plane deformation in the macrocycle. The spectral band at ~1453 cm^{-1} is due to the stretching vibrations of the isoindole ring, and the bands at ~1648 cm^{-1} correspond to the C−N in-plane stretching vibration (Figure 6) [20,21].

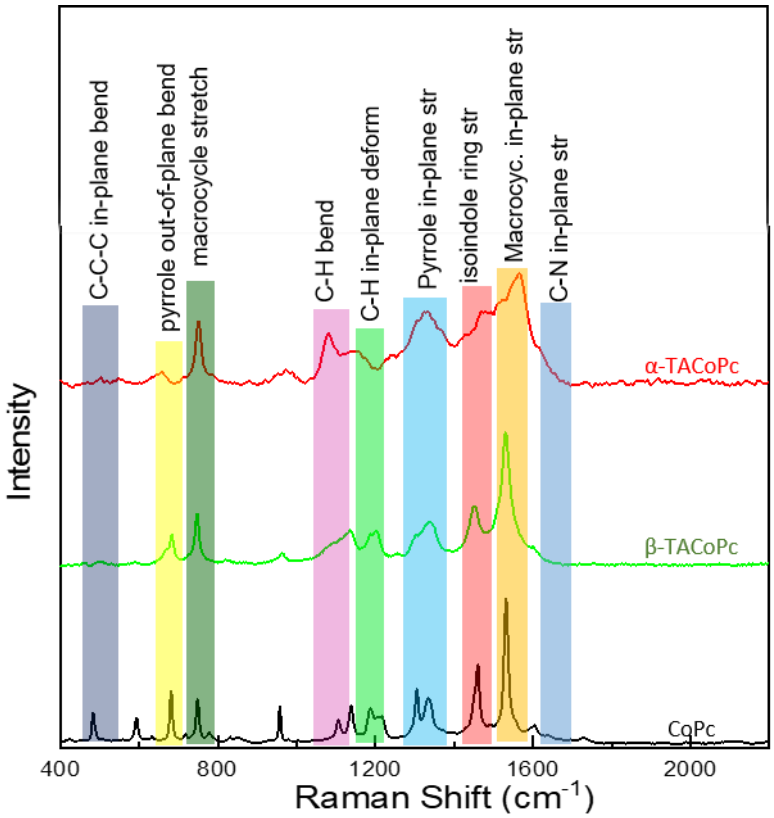

Figure 6 Raman Spectra of pristine electrocatalysts

NMR spectroscopy was done using α- and β-Tetraamino Zinc Phthalocyanine (prepared by the same synthesis route with the metal salt replaced with Zn salt) to confirm the position of functionalization for each synthesised isomer. TAZnPc was used since Co(II) is paramagnetic and therefore cannot be used for NMR characterization. As seen in Fig. 7(a), α-isomer shows split peaks for the 2 N-H protons around 7.26-7.4, implying that they are no longer chemically equivalent. This is due to one of them H-bonding with the nitrogen atom on the macrocycle forming a stable six-membered ring, hence limiting the free rotation of NH_2 about the C-N bond. [22] The signal due to the proton having two neighbouring protons is observed as a multiplet around 8.55. In the case of β-isomer, the two N-H protons are chemically equivalent as seen from the single signal ~6.3, and there is no triplet peak since none of the protons in the structure has more than one neighbour to split its signal.

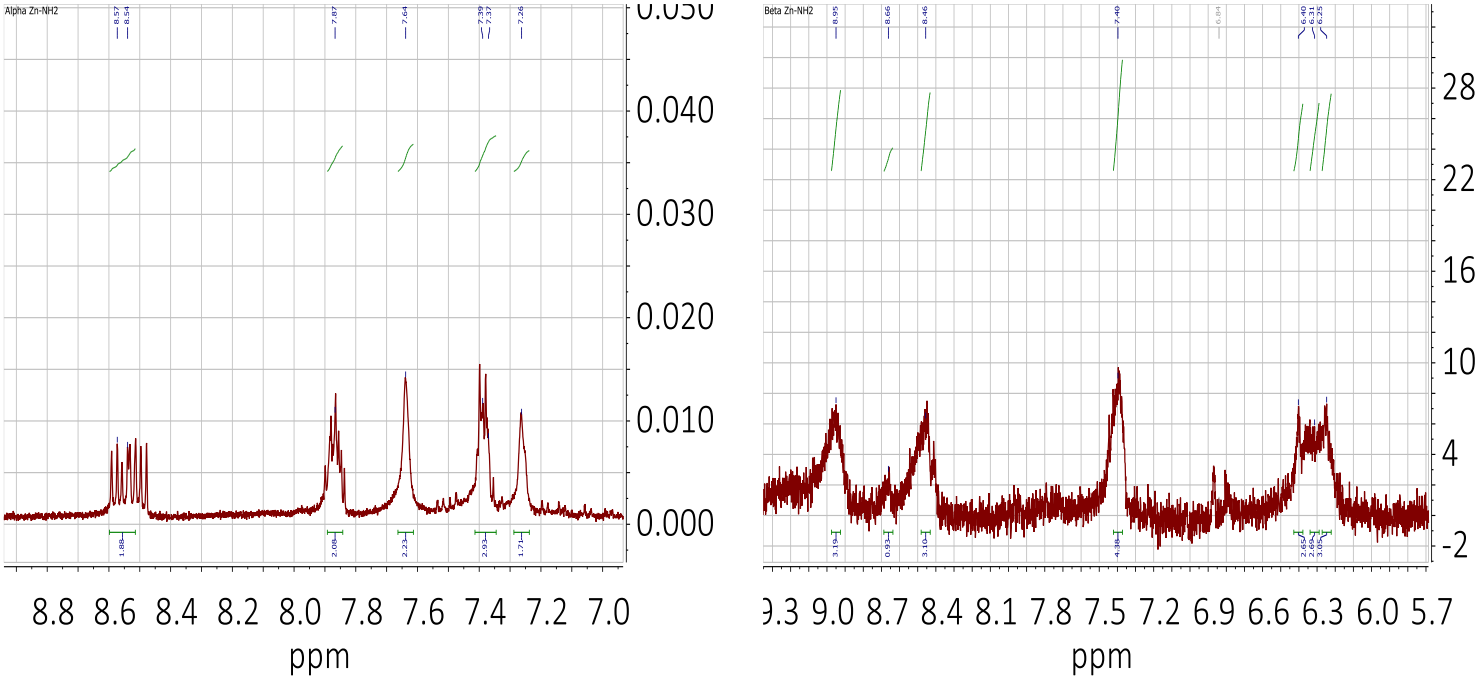

Figure 7 Proton NMR Spectra of (a) α-TAZnPc and (b) β-TAZnPc

3.2 TACoPc/CNT Composites

As it is well known that electron transfer to and from the catalyst is enhanced by CNT, the composite of the molecular electrocatalyst with CNT was prepared for investigating the electrochemical oxidation of hydrazine. α- TACoPc, β-TACoPc, and CoPc anchored on CNT (α-TACoPc/CNT, β-TACoPc/CNT, CoPc/CNT) were characterized by UV−visible, ATR-FTIR, Raman spectroscopy, FESEM and EDS elemental analysis.

UV−vis spectrum (Figure 8a) of the composite catalytic system shows the presence of Soret and Q-bands, attesting to the successful fusion of Pcs onto CNT. Both the characteristic IR signals of the CNT in the TACoPc/CNT composite system and the corresponding Phthalocyanine ring features are noticeable in the FTIR spectra (Figure 8b). The Raman spectra (Figure 8c) show the presence of the defect band and

graphitic band characteristic to carbon nanotubes in pure CNT as well as the composite catalysts [6,23]. But the Pc signals are all masked (since their concentration is low compared to nanotubes in the composite system) by these highly intense signals. The I_D/I_G (defect band intensity/graphitic band intensity) ratio in the CNT still increases a significant amount upon going from CNT to CoPc/CNT and TACoPc/CNTs, in agreement with the literature, [6,23] implying successful combination. These characterization techniques verify the presence of CNT and TACoPc isomers as part of the electrocatalytic architecture.

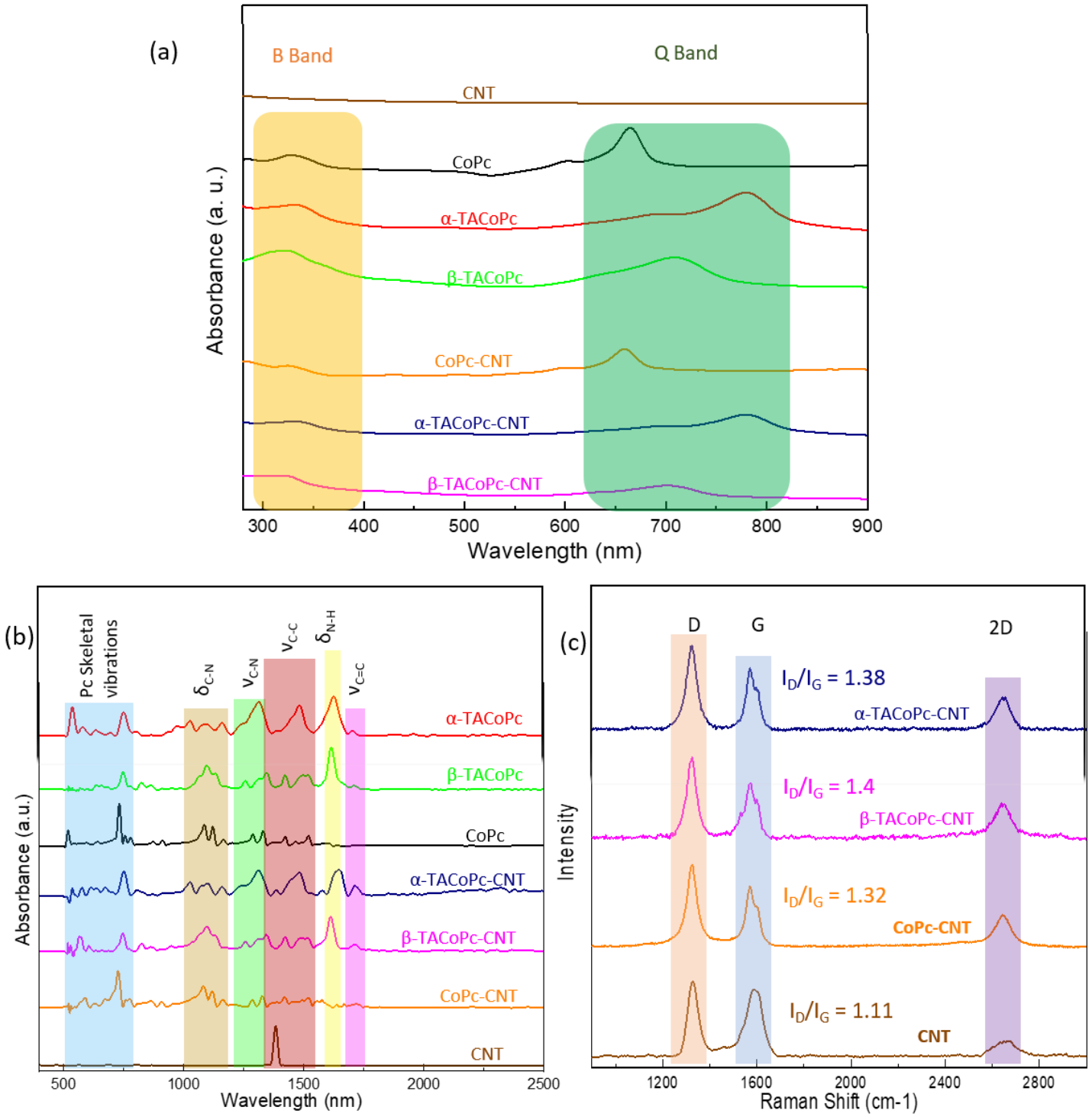

Figure 8 (a) UV-vis spectra, (b) FTIR spectra, and (c) Raman spectra of CoPc-CNT, α-TACoPc-CNT and β-TACoPc-CNT

The CNT-TACoPc composites were further characterized by FESEM for morphology and elemental analysis. The tubular morphology of carbon nanotubes was clearly observed in the FESEM images. The composite catalysts have Co, N and C according to the EDX pattern. The percentage of Co and N observed in both the TACoPc/CNT isomers was approximately similar.

α-TACoPc/CNT

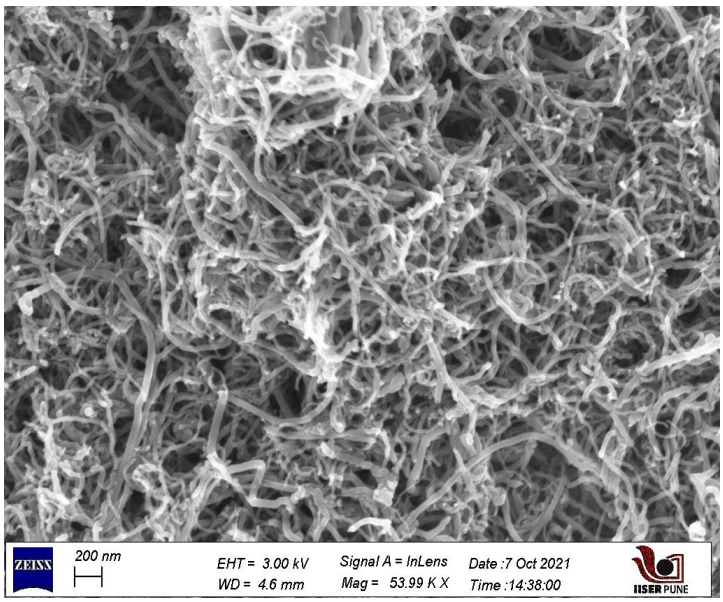

β-TACoPc/CNT

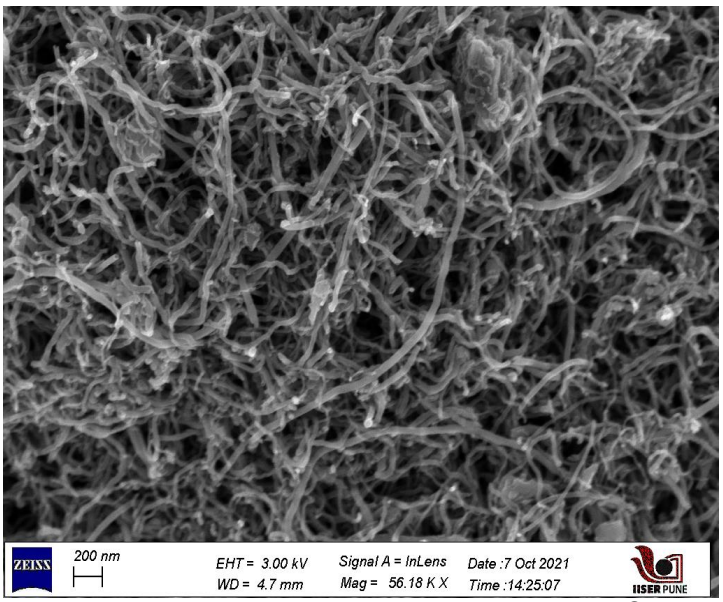

CoPc/CNT

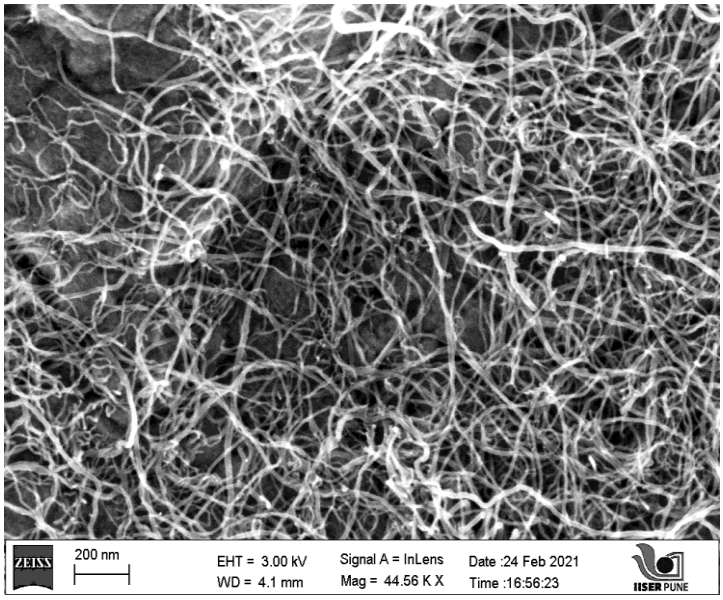

CNT

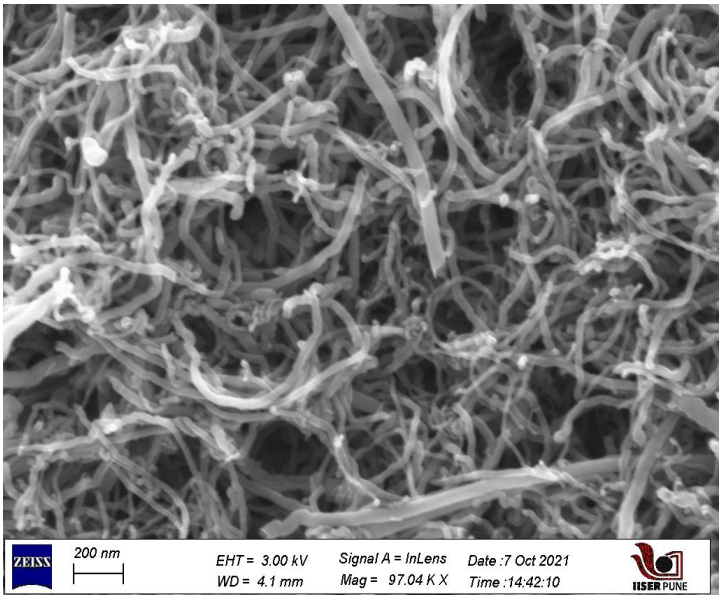

Figure 9 FESEM Images of CNT and CNT composite catalyst

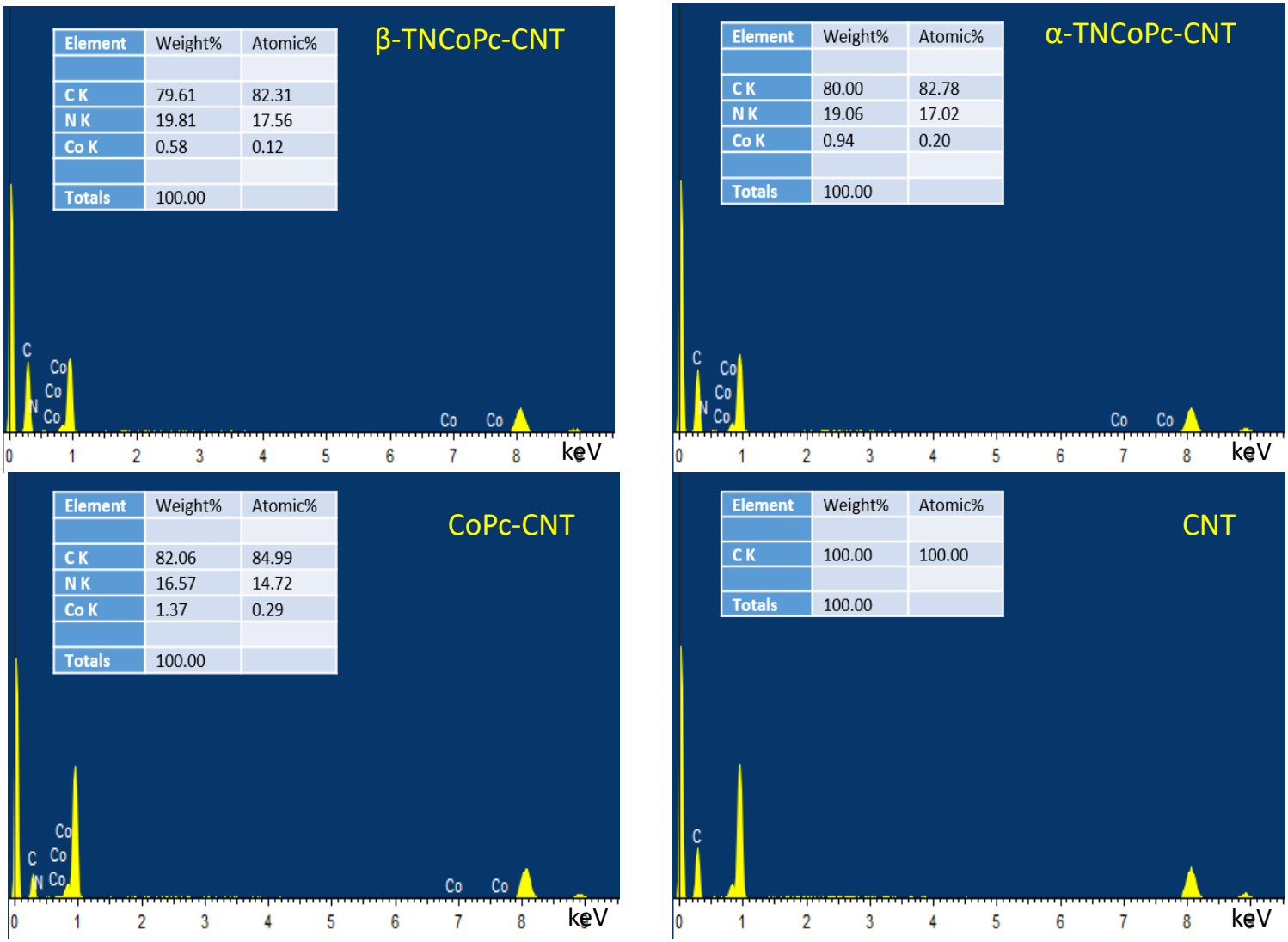

Figure 10 EDX spectra of CNT and CNT composite catalyst

Chapter 4 : Results and Discussion

4.1 Voltammetry

For studying catalytic activity towards hydrazine oxidation, linear sweep voltammetry was performed with glassy carbon working electrodes modified with each TACoPc/CNT composite catalyst from -0.3V to +1.2V vs RHE in the presence of hydrazine in 0.1M KOH.

As observed in Figure 11, all of the catalysts give rise to an oxidation peak in the voltammogram, which means that both tetraamino isomers and CoPc can catalyse the oxidation reaction. However, the onset potential and the peak current are different for all three. Among the isomers, β-TACoPc was observed to perform better than α-TACoPc and CoPc towards hydrazine oxidation since it has the lowest onset potential and highest current. α-TACoPc seems to start catalysing the reaction around the same potential as CoPc, but reaches a higher peak current.

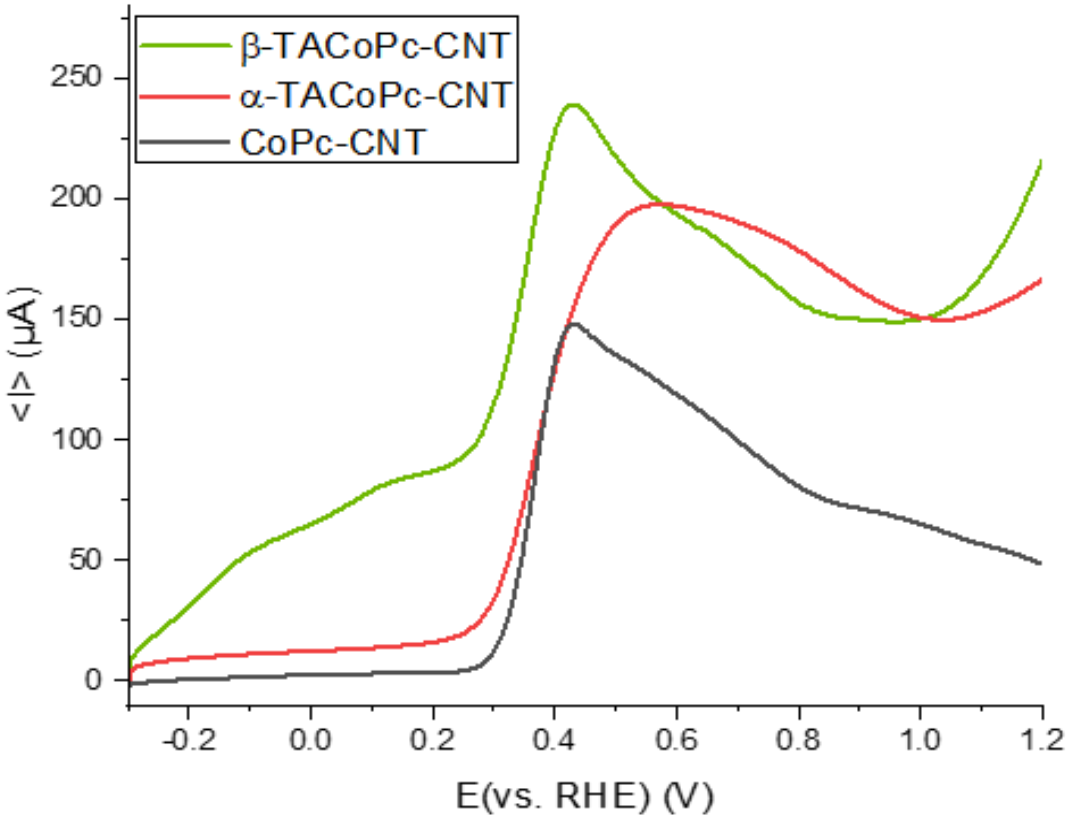

Figure 11 Comparison of linear sweep voltammogram for hydrazine oxidation with β-TACoPc/CNT, α-TACoPc/CNT, and CoPc/CNT. Scan rate:50mV/s, Concentration:3.5mM Hydrazine in 0.1M KOH

We further carried out the scan rate (Figure 13) and concentration dependence (Figure 12) studies on all three composite catalytic systems. The concentration of hydrazine in the system was increased by 0.5mM after each linear scan voltammogram recorded at a scan rate of 50mV/s. Similarly, LSVs for each catalyst

were recorded in a system containing 5mM hydrazine at different scan rates for studying scan rate dependence. The peak current was observed to be linearly proportional to the concentration of hydrazine, confirming that the current is due to the electrocatalytic oxidation of hydrazine on the synthesized catalyst. The scan rate dependence studies display that the peak current is linearly proportional to the square root of scan rate ($v^{1/2}$) (Figure 13(d)). The logarithmic plot (Figure 13(e)) also suggests a linear relationship between the two suggesting that the reaction follows diffusion-controlled kinetics.

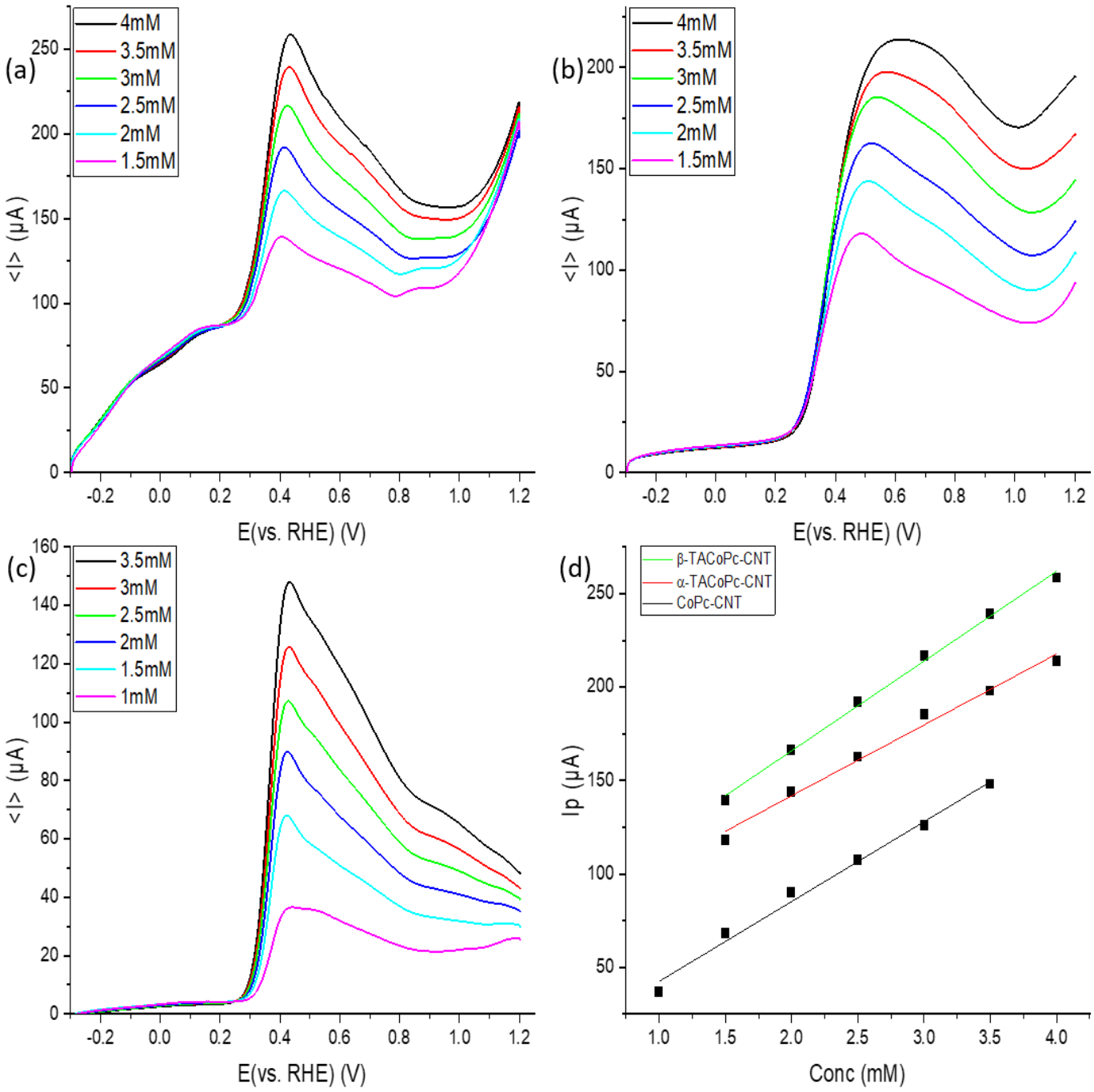

Figure 12 Concentration dependence study of (a) β-TACoPc/CNT, (b) α-TACoPc/CNT, and(c) CoPc/CNT. (d) I_p vs c plot

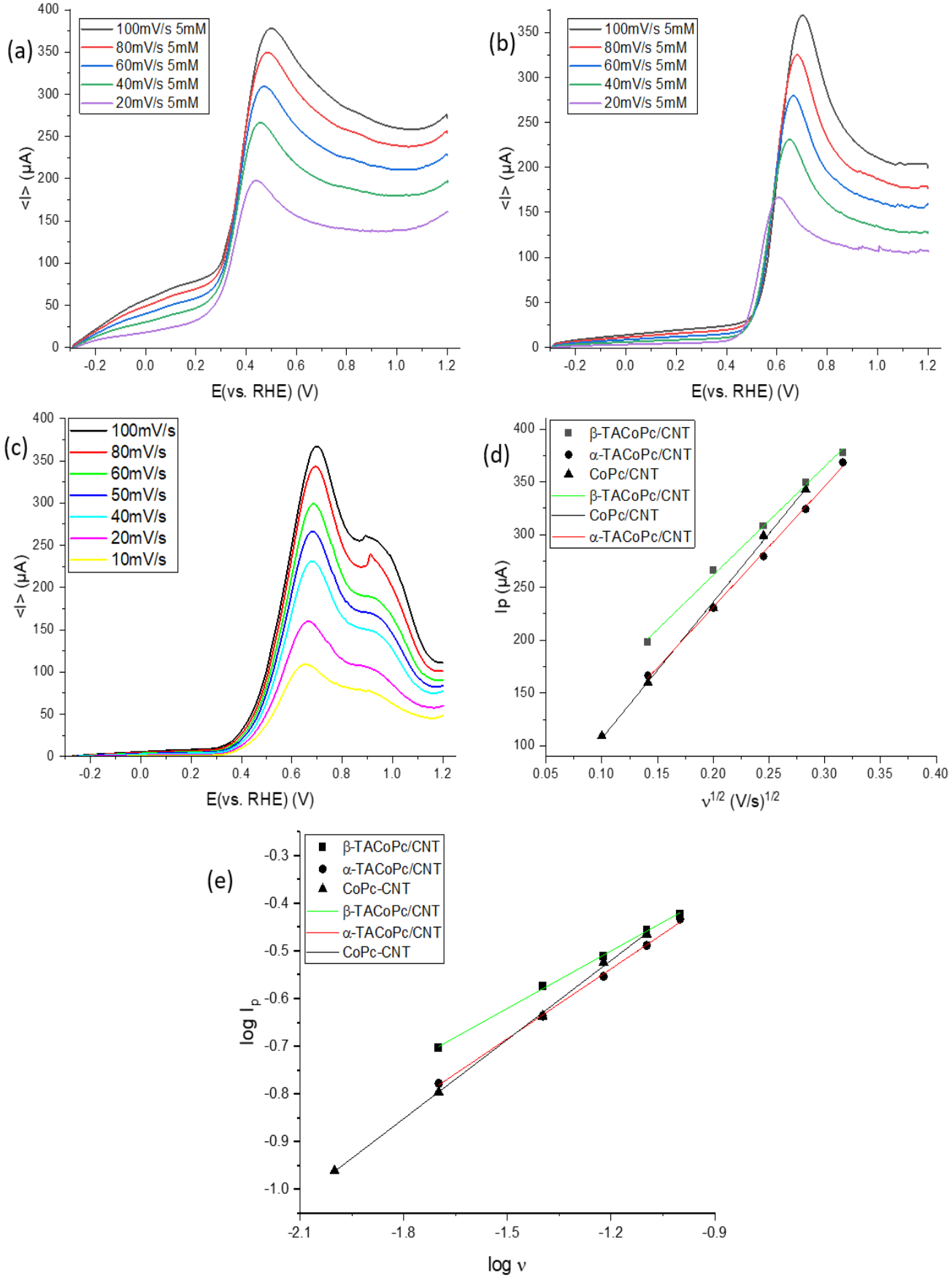

Figure 13 Scan rate dependence study of (a) β-TACoPc/CNT, (b) α-TACoPc/CNT, and(c) CoPc/CNT. (d) I_p vs $v^{1/2}$ plot and (e) log I_p (A) vs log v plot

The stability of the catalysts was studied with chronoamperometry, where a specific constant potential is applied across the electrode and then the current response is recorded. The applied potential was chosen to be the potential at a point before the half-wave potential in the corresponding cyclic voltammogram of each catalyst. The chronoamperogram (Figure 13(a)) shows that the current has stabilised to a certain value for both catalysts towards the end of 6 hours. This stable current is quite close to the current recorded in the cyclic voltammogram (Figure 13(b)) corresponding to the applied potential, implying that the catalysts exhibit long term stability.

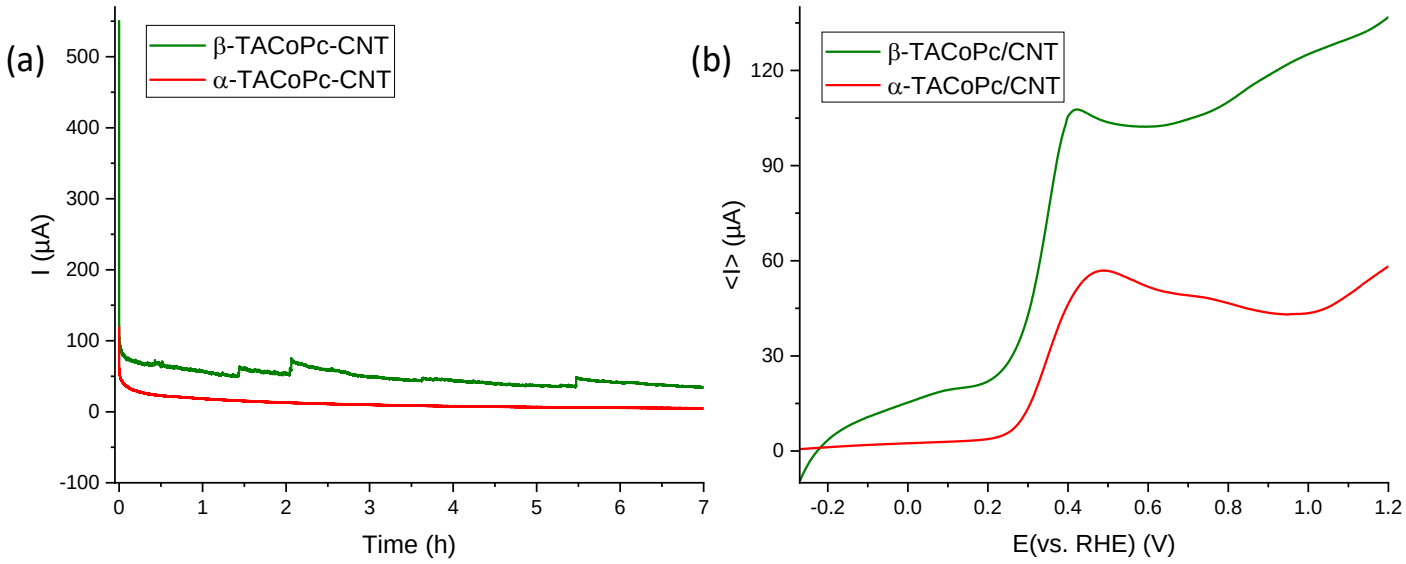

Figure 14 (a)Chronoamperometry of TACoPc/CNT composite drop-casted on to GC electrode. Electrolyte used was 3 mM Hydrazine in 0.1 M KOH and the potential applied was -300mV for β-TACoPc and -285mV for α-TACoPc, (b)cyclic voltammogram recorded in the same condition at scan rate 10 mV/s

In order to show that the reaction is catalysed by the molecular catalyst and not the CNT support, we have prepared the Self-assembled monolayer (SAM) electrodes of the pristine electrocatalysts and studied their electrocatalytic activity towards hydrazine by Linear sweep voltammetry (Figure 15). The same behaviour was

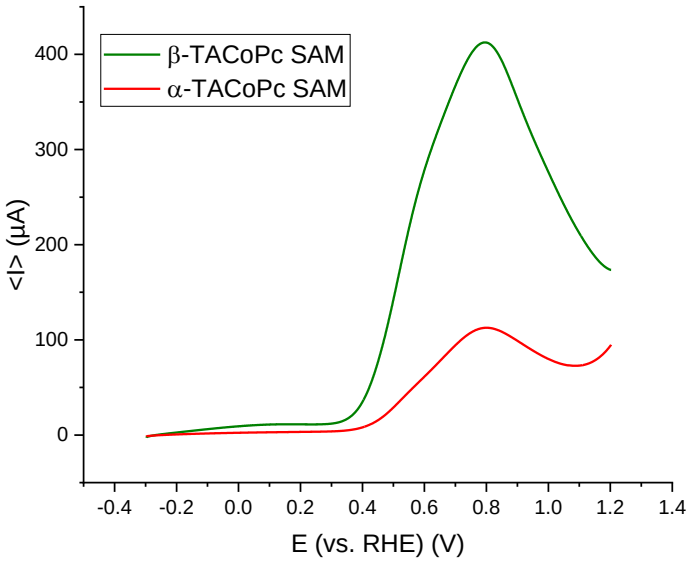

Figure 15 Hydrazine oxidation by pristine TACoPc isomers self-assembled into a monolayer on the GC electrode. Conc-10mM Hydrazine in 0.1 M KOH, Scan rate- 100 mV/s

exhibited as in the case of the CNT composites, with β-TACoPc giving a lower onset potential as well as higher current. Hence, we can conclude that the electrocatalytic behaviour towards hydrazine oxidation is solely contributed by the TACoPc isomers and does not stem from CNT. After studying the hydrazine oxidation on these electrocatalytic molecules we investigated their performance in the fuel cell application.

4.2 Fuel Cell Data

The fuel cell was assembled in a flooded cell asymmetric electrolytic configuration, as discussed in the experimental chapter. The I-V characteristics curve for the fuel cells assembled (Figure 16) exhibits a better performance with higher cell potential as well as greater power density for the one based on α-TACoPc/CNT when compared to β-TACoPc/CNT. Both the isomeric molecules exhibited decent fuel cell performance, with the β isomer outperforming the α isomer.

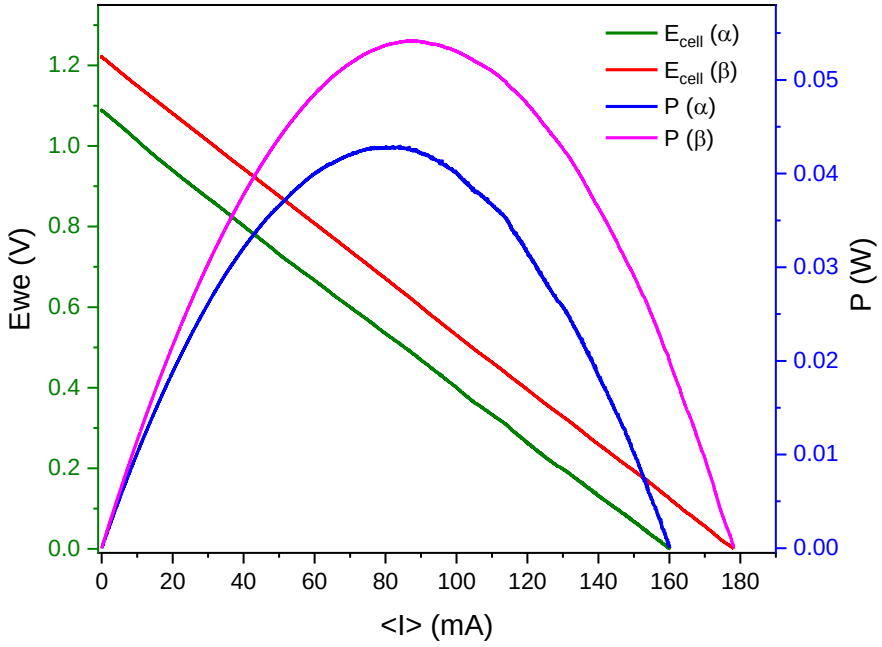

Figure 16 Polarisation curve comparison for Hydrazine-O_2 acid-base fuel cell using α-TACoPc/CNT and β-TACoPc/CNT electrocatalysts.

One of the important parameters for fuel cell performance is the stability and durability of the catalyst in the real fuel cell configuration. To study that, we have carried out the long term constant current test (Figure 17) with both the isomeric molecules. The α isomer-based fuel cell exhibits higher efficiency and durability as compared to the β isomer-based fuel cell.

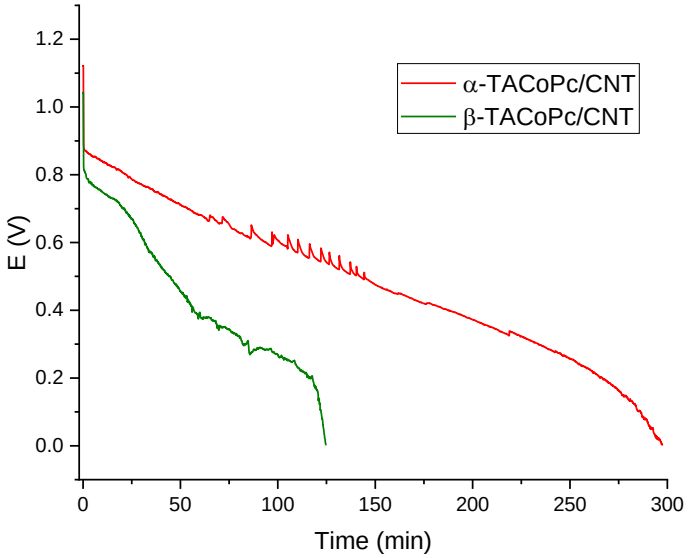

Figure 17 Constant Current profile for Hydrazine-O_2 fuel cell

Conclusion

We have studied the electrocatalytic activity of Tetraamino Cobalt Phthalocyanine and the effect of isomerism on the same via the electrochemical oxidation of hydrazine. The TACoPc isomer catalysts were synthesized according to literature and characterized by several spectroscopic techniques. It was found that β-TACoPc serves as a better electrocatalyst for hydrazine oxidation over α-TACoPc and CoPc. They were then used to make a fuel cell with oxygen reduction in acid as the cathodic reaction, and the performance of each isomer-based fuel cell was monitored. The fuel cells using both isomers displayed adequate performance with β showing better performance and α showing more stability.

References

1. C. Costentin, J. M. Savéant, *Nat. Rev. Chem.* **2017**, *1*, 1–8.
2. S. Mukhopadhyay, A. R. Kottaichamy, Z. M. Bhat, N. C. Dargily, M. O. Thotiyl, *Electroanalysis* **2020**, *32*, 2387
3. Zagal, J. H.; Griveau, S.; Silva, J. F.; Nyokong, T.; Bedioui, F. *Coord. Chem. Rev.* **2010**, *254*, 2755–2791.
4. C. Li, T. Huang, Z. Huang, J. Sun, C. Zong, J. Yang, W. Deng and F. Dai, *Dalton Trans.* **2019**, *48*, 17258–17265
5. Wang M., Torbensen K., Salvatore D., Ren S., Joulié D., Dumoulin F., Mendoza D., Lassalle-Kaiser B., Işci U., Berlinguette C. P., Robert M., *Nat. Commun.* **2019**, *10*, 3602
6. Kottaichamy, A. R.; Begum, S.; Nazrulla, M. A.; Dargily, N. C.; Devendrachari, M. C.; Bhat, Z. M.; Thimmappa, R.; Makri Nimbegondi Kotresh, H.; Vinod, C. P.; Thotiyl, M. O. *J. Phys. Chem. Lett.* **2020**, *11*, 263– 271.
7. Kottaichamy, A. R.; Begum, S.; Devendrachari, M. C.; Bhat, Z. M.; Thimmappa, R.; Makri Nimbegondi Kotresh, H.; Vinod, C. P.; Thotiyl, M. O. *Anal. Chem.* **2020**,*92 (6),* 4541-4547
8. Therdthianwong, A.; Saenwiset, P.; Therdthianwong, S. *Fuel* **2012**, *91 (1)*, 192–199.
9. Hsieh, C. Y.; Nguyen, X. V.; Weng, F. B.; Kuo, T. W.; Huang, Z. M.; Su, A. *Int. J. Electrochem. Sci.* **2016**, 11 (12), 10449–10461.
10. San Martin, J. I.; Zamora, I.; San Martin, J. J.; Aperribay, V.; Torres, E.; Eguia, P. *Energy* **2010**, *35 (5),* 1898–1907.
11. Mann, R. F.; Amphlett, J. C.; Hooper, M. a. I.; Jensen, H. M.; Peppley, B. a.; Roberge, P. R. *J. Power Sources* **2000**, *86 (1–2)*, 173–180
12. Soloveichik, G. L. *Beilstein J. Nanotechnol.* 2014, *5 (1)*, 1399–1418.
13. Ding, Y., Cai, P., & Wen, Z. *Chem. Soc. Rev.* **2021***, 50(3), 1495–1511.*
14. Al-lami, A. K.; Majeed, N. N.; Al-mowali, A. H. *Chem. Mater. Res.* **2013**, *3 (4),* 59−68.
15. Cao, R.; Thapa, R.; Kim, H.; Xu, X.; Gyu Kim, M.; Li, Q.; Park, N.; Liu, M.; Cho, J. *Nat. Commun.* **2013**, *4 (May)*, 2076.

16. Agilent Te. UV-Visible Spectroscopy. *R. Soc. Chem*. **2000**, *Agilent Te*, 22.
17. N. Elgrishi; K.J. Rountree; B.D. McCarthy; E.S. Rountree; T.T. Eisenhart; J.L. Dempsey. *J. Chem. Educ.* **2018**, *95,* 197–206
18. Chen, C.; Levitin, G.; Hess, D. W.; Fuller, T. F. *J. Power Sources* **2007**, *169 (2)*, 288–295.
19. A. B. P. Lever, S. R. Pickens, P. C. Minor, S. Licoccia, B. S. Ramaswamy, and K. Magnell. *J. Am. Chem. Soc.* **1981**, *103*, 6800-6806.
20. R. Georgescu, C. Boscornea, I. Calinescu, R. State. *New J. Chem.* **2004**, *28,* 676-680.
21. Lokesh, K. S.; Adriaens, A. *Dye. Pigment*. **2013**, *96 (1)*, 269–277.
22. Xian-Fu Zhang, Xijiang Li, Lihong Niu, Lou Sun, Lu Liu. *J Fluoresc* **2009**, *19*, 947–954
23. Zhang, X.; Wu, Z.; Zhang, X.; Li, L.; Li, Y.; Xu, H.; Li, X.; Yu, X.; Zhang, Z.; Liang, Y.; et al. *Nat. Commun.* **2017**, *8 (March)*, 14675.